The Astrophysical Journal, 721:576–581, 2010 September 20 doi:10.1088/0004-637X/721/1/576

MEASUREMENT OF THE RADIATIVE DECAY RATE OF THE METASTABLE $(2s^2 2p^5_{3/2} 3s_{1/2})_{(J=2)}$ LEVEL IN Fe XVII

J. R. Crespo López-Urrutia[1] and P. Beiersdorfer
Lawrence Livermore National Laboratory, 7000 East Avenue, Livermore, CA 94550, USA
Received 2009 June 23; accepted 2010 July 27; published 2010 August 30

ABSTRACT

The radiative decay rate of the $(2s^2 2p^5_{3/2} 3s_{1/2})_{J=2} \rightarrow (2s^2 2p^6)_{J=0}$ transition was measured in Ne-like Fe XVII. This transition forms the prominent magnetic quadrupole line, dubbed $M2$ or $3H$, in the Fe XVII spectrum at 17.10 Å. Different theoretical models predict radiative rates for this transition that diverge by almost a factor of 2, making intensity predictions for this line uncertain in environments where it is affected by de-excitation due to either electron-impact collisions or photoionization. Our result of $(2.04^{+0.03}_{-0.09}) \times 10^5$ s^{-1} is very close to the value of 2.06×10^5 s^{-1} predicted by the Flexible Atomic Code.

Key words: atomic data – atomic processes – line: formation – X-rays: general

Online-only material: color figures

1. INTRODUCTION

The Fe XVII spectrum has been a very important diagnostic of astrophysical objects observed with the *Chandra* and *XMM-Newton* X-ray Observatories (Paerels & Kahn 2003). Iron is abundant in many objects, and because of its closed-shell nature the Fe^{16+} ion is the most abundant charge state over a wide temperature range. The Fe XVII spectrum is typically dominated by the two strong $3d \rightarrow 2p$ lines, commonly labeled $3C$ and $3D$, and by the three $3s \rightarrow 2p$ transitions, commonly labeled $3F$, $3G$, and $M2$. The $M2$ line has also been dubbed $3H$ in early observations of the Sun (Parkinson 1973; Loulergue & Nussbaumer 1975).

Despite effort that started decades ago (Loulergue & Nussbaumer 1973; Smith et al. 1983) spectral modeling calculations of Fe XVII have had difficulties providing synthetic spectra that matched the observations from many sources observed with the *Chandra* and *XMM-Newton* X-ray Observatories (Xu et al. 2002; Behar et al. 2001; Ness et al. 2003; Gu 2009). One early, targeted laboratory observation of the Fe XVII spectrum using an electron beam ion trap had found agreement with two spectral models (Laming et al. 2000); however, the laboratory data did not agree with astrophysical observations. Notably, the ratio of the $3s \rightarrow 2p$ to $3d \rightarrow 2p$ intensities measured in the laboratory, while matching theory very nicely, was considerably smaller than the ratio observed in essentially all collisional astrophysical sources, including the Sun, stellar coronae, and clusters of galaxies. Subsequent targeted laboratory measurements of Fe XVII, by contrast, found values for the $3s \rightarrow 2p$ to $3d \rightarrow 2p$ intensity ratios that were considerably higher than those from these early measurements over a wide range of collision energies (Beiersdorfer et al. 2002; Brown 2008). For example, at an electron collision energy of 0.9 keV the ratio of intensity of the summed $3F$, $3G$, and $M2$ lines to that of the $3C$ line measured by Beiersdorfer et al. (2002) was 1.57 times higher than that measured by Laming et al. (2000).[2] The newer measurements thus contradicted the early laboratory results, and they were now in partial agreement with the solar and astrophysical data. Subsequently, laboratory measurements using thermal plasmas were in excellent agreement with solar and astrophysical spectra (Beiersdorfer et al. 2004). The newer measurements, by extension, were in little agreement with the spectral models existing at the time. Similarly, poor agreement between laboratory data and astrophysical spectral models has also been seen in Ni XIX (Brown et al. 2001; Gu et al. 2004; Chen et al. 2006, 2007).

Inaccuracies in the radiative decay rates assumed in the models are one source of potential problems that may affect the predictive quality of spectral calculations. The $(2s^2 2p^5_{3/2} 3s_{1/2})_{J=2} \rightarrow (2s^2 2p^6)_{J=0}$ transition, which forms one of the prominent $3s \rightarrow 2p$ lines, has a low radiative decay rate because it is forbidden to proceed by an electric-dipole transition. In fact, it is also forbidden to de-excite by magnetic dipole and electric quadrupole decay. The first allowed higher-order multipole is magnetic quadrupole decay, hence its common label $M2$. As a result, the $(2s^2 2p^5_{3/2} 3s_{1/2})_{J=2}$ upper level has a rather long lifetime, which makes its intensity susceptible to de-excitation by electron-impact collisions or by exposure to a strong photon flux, diminishing its intensity. Such de-excitation has been observed in the spectra from various astrophysical sources, e.g., the magnetic cataclysmic variable star Ex Hya (Mauche et al. 2001; Mauche et al. 2005). Theoretical predictions for the upper level lifetime (Smith et al. 1983; Bhatia & Doschek 1992; Cornille et al. 1994; Safronova et al. 2001; Nahar et al. 2003) vary by almost a factor of 2, from 4 μs to 7 μs, as shown in Table 1. Because radiative rates are inherent components of collisional-radiative models used for predicting synthetic spectra, uncertainties in the predicted radiative decay rates compromise the accuracy of spectral predictions.

A laboratory measurement of the radiative decay rates of the Fe XVII lines in general, and of the $(2s^2 2p^5_{3/2} 3s_{1/2})_{J=2} \rightarrow (2s^2 2p^6)_{J=0}$ transition in particular, is warranted to distinguish among theoretical calculations and, in turn, to improve the spectral models. No measurement has yet been performed to determine the radiative decay rate of magnetic quadrupole transitions in any highly charged neon-like ion. Thus, there has been no experimental guidance to choose among the calculational approaches used to predict the Fe XVII spectrum. Because the lifetime of the $(2s^2 2p^5_{3/2} 3s_{1/2})_{J=2}$ upper level

[1] Current address: Max-Planck-Institut für Kernphysik, Saupfercheckweg 1, D-69117 Heidelberg, Germany.

[2] This discrepancy was found by comparing the raw data from both measurements before applying corrections for angular anisotropy effects due to X-ray line polarization; the discrepancy persists after such corrections are made.

Table 1
Calculated and Measured Values for the Radiative Lifetime of the $(2s^2 2p^5_{3/2} 3s_{1/2})_{J=2}$ Level in Fe XVII

Authors	Value (μs)
Calculation	
Bhatia et al. (1985)	4.03
Bhatia & Doschek (1992)	5.92
Bhatia & Saba (2001)	5.92
Bhatia & Doschek (2003)	4.79
Cornille et al. (1994)	7.17
FAC (present calculation)	4.85
Loulergue & Nussbaumer (1975)	4.95
Mauche et al. (2001)	4.76
Nahar et al. (2003)	4.44
Safronova et al. (2001)	5.46
Measurement	
Present measurement	$4.91^{+0.23}_{-0.08}$

is in the microsecond range for iron, most methods used to study radiative decay rates, employing, for example, the beam-foil technique, Kingdon traps, or ion-storage rings, cannot be employed, as they are applicable only for much shorter or much longer lifetimes (Träbert 2002). The electron beam ion trap technique is currently the only technique that can produce reliable results in the microsecond range (Träbert 2008). This technique, in fact, enables measurements in the nanosecond to millisecond range (Wargelin et al. 1993). The technique has already been employed to determine several astrophysically relevant lifetime measurements (Stefanelli et al. 1995; Crespo López-Urrutia et al. 1998; Träbert et al. 1999, 2000; Neill et al. 2000; Beiersdorfer et al. 2003b; Lapierre et al. 2005; Crespo López-Urrutia et al. 2006; Brenner et al. 2007; Träbert 2008). The electron beam ion trap technique has been employed to perform the present measurement of the radiative decay rate of the $(2s^2 2p^5_{3/2} 3s_{1/2})_{J=2} \rightarrow (2s^2 2p^6)_{J=0}$ transition.

2. THEORY

In a plasma, essentially all energy levels can be populated. The experimental conditions in an electron beam ion trap, however, make it possible to ignore energy levels higher than those displayed in Figure 1. The reason is that excitation in an electron beam ion trap is practically limited to those levels with energy equal to or less than the energy of the electrons in the beam.

A 37 level collisional-radiative model generated by the Flexible Atomic Code (FAC) version 1.1.1 (Gu 2008) was used to estimate the population distribution under the given conditions. This model comprises the ground level and all 36 excited states with a valence electron in the $n = 3$ shell. The main mechanism (>90%) for populating the $(2s^2 2p^5_{3/2} 3s_{1/2})_{J=2}$ level with a beam of electrons with energy near 800 eV, i.e., about 70 eV above the threshold for electron-impact excitation of the $(2s^2 2p^5_{3/2} 3s_{1/2})_{J=2}$ level, is direct electron-impact excitation of the $2s^2 2p^5 3p$ levels followed by radiative cascades of dipole-allowed transitions. Direct excitation of the $3s$ levels is less important (<10%), because the cross sections for direct electron-impact excitation of the $3p$ levels are considerably higher than those of the $3s$ levels (Beiersdorfer et al. 1990). The electric-dipole transitions between $3p$ and $3s$ are very fast ($A_{ik} \approx 10^{11}$ s^{-1}), transferring the $3p$ electron to the levels from which the lines $3F$, $3G$, and $M2$ arise. When the electron beam energy is below the threshold for electron-impact excitation, no

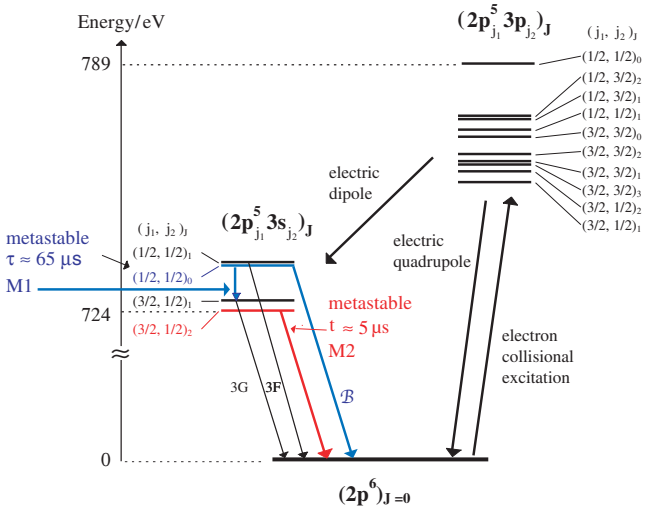

Figure 1. Grotrian diagram of the $2s^2 2p^6$, $2s^2 2p^5 3s$, and $2s^2 2p^5 3p$ levels of neon-like Fe XVII. Lifetime values shown are theoretical predictions using FAC. (A color version of this figure is available in the online journal.)

excitation of the neon-like lines can take place. We note that recombination of iron ions in the next higher charge state, Fe^{17+}, cannot populate the levels under consideration either. This process is active in hot collisional plasma, but does not play a role in our laboratory measurements because no Fe^{17+} ions are produced under the present experimental conditions.

3. EXPERIMENT

The Livermore EBIT-II electron beam ion trap (Beiersdorfer 2008) was employed for the present measurements. Here, an electron beam of well defined energy is launched axially into the 3 T magnetic field of a superconductive Helmholtz coil. In the region of highest magnetic field, the beam is compressed to a diameter of about 50 μm for a length of 2 cm (Levine et al. 1989). The radial field produced by the space charge of the beam attracts positive ions. Three cylindrically shaped drift tubes define an axial electrical field with a minimum in the middle, which confines the ions in their axial movement. The trapped ions are sequentially stripped of their electrons by collisions with beam electrons up to a charge state whose ionization potential is commensurate with the energy of the electron beam.

The measuring cycle starts with the firing of a metal vapor vacuum arc (MeVVA) ion source (Brown et al. 1986). The arc generates Fe ions with low charge states. Those ions are injected axially into the trap by traversing an accelerating potential step. The potential of the top drift tube is then lowered to allow entry into the trap region. The beam energy is set to reach the desired charge state, which for Fe^{16+} is reached in a few milliseconds. Charge exchange with the residual gas, radiative recombination involving beam electrons, and electron-impact collisional ionization are the main processes determining the ionization balance.

The beam energy is determined by the potential difference between the electron gun cathode and the central drift tube of the trap, in addition to a correction for the beam space charge in the trap. Usually, the electron gun is at ground potential, and the drift tube is at a positive potential. To change the electron beam energy, the high-voltage floating rack, which is connected to the drift tube assembly, is switched between different values.

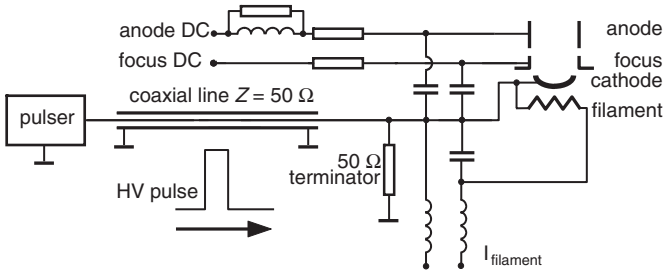

Figure 2. Simplified electrical wiring diagram of the high voltage pulser and the electron gun of EBIT-II for fast electron energy switching. A short (tens of microseconds) square high voltage pulse raises the cathode potential by +170 V, thus lowering the electron beam energy by the same amount.

This allows only a limited slew rate due to the large capacity of the rack and would be too slow to perform the measurements presented in this paper.

For faster switching of the beam energy, the electron gun was modified, as shown in Figure 2, and separated from ground by means of a high power (200 W) coaxial 50 Ω terminator at the end of a $Z = 50$ Ω transmission line. The *e*-gun cathode, heating filament, focus electrode, and extraction anode were connected to each other by appropriate low-inductance capacitors to provide low impedance paths between them for the high frequency components of the switching pulse, while keeping constant the DC potential differences necessary for *e*-gun operation and beam focusing. In this way, the potential of the whole electron gun could be pulsed without major changes in its emission characteristics. A square pulse of 6 ns rise time and several μs duration produced by a high voltage pulser propagated along the transmission line and raised the potential of the *e*-gun. The pulse shape was not much distorted, as oscilloscopic measurements showed, and the pulse rise time only marginally deteriorated.

We changed the electron beam energy between the value needed for the excitation of the $2s^22p^53p$ levels of Ne-like Fe (about 800 eV) and the value needed to cease excitation of the $2s^22p^53s$ levels by pulsing the electron gun potential from ground to +170 V for 20 μs. In order to collect signal at a reasonable rate, pulsing of the gun assembly was carried out with a repetition rate of 15 kHz. The +170 V voltage pulse was sufficient to drop the beam energy to 630 eV. This is sufficiently low to stay clear of exciting dielectronic recombination satellite transitions (Beiersdorfer 2003). We also performed experiments in which we completely turned off the electron beam as reported earlier (Crespo López-Urrutia et al. 2006).

A flat-crystal spectrometer with high resolution ($\lambda/\Delta\lambda \approx 600$; Beiersdorfer & Wargelin 1994) and a Si(Li) solid-state detector were used to monitor the radiation from the ions in this experiment. Synchronously with the phase of the voltage pulse on the *e*-gun assembly, each X-ray photon arriving at one of the two detectors was recorded by an event-mode data collection system. A synchronized voltage sawtooth ramp was generated with each pulse. The voltage value of the ramp was sampled and digitized at the arrival time of each photon. The timing between *e*-gun voltage pulse and arrival time of each photon was so registered, together with the photon energy, for each detector.

An independent determination of the time response of the beam energy based on the time response of the emission of line $3F$ yielded a rise time better than 18 ns limited only by the detector rise time, as illustrated in Figures 3 and 4. In Figure 3, we show the time evolution of the total intensity of the transitions $3F$, $3G$, and $M2$ recorded with the flat-crystal

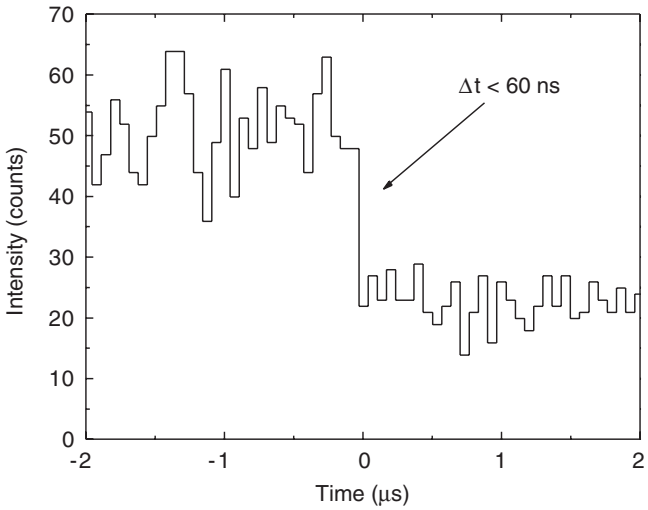

Figure 3. Total signal strength recorded with the crystal spectrometer while switching the electron beam energy from a value above the threshold for direct excitation of the $2p^6$–$2p^53s$ transitions to a value well below the threshold. The time resolution is limited here by the digitizer time step size of about 60 ns.

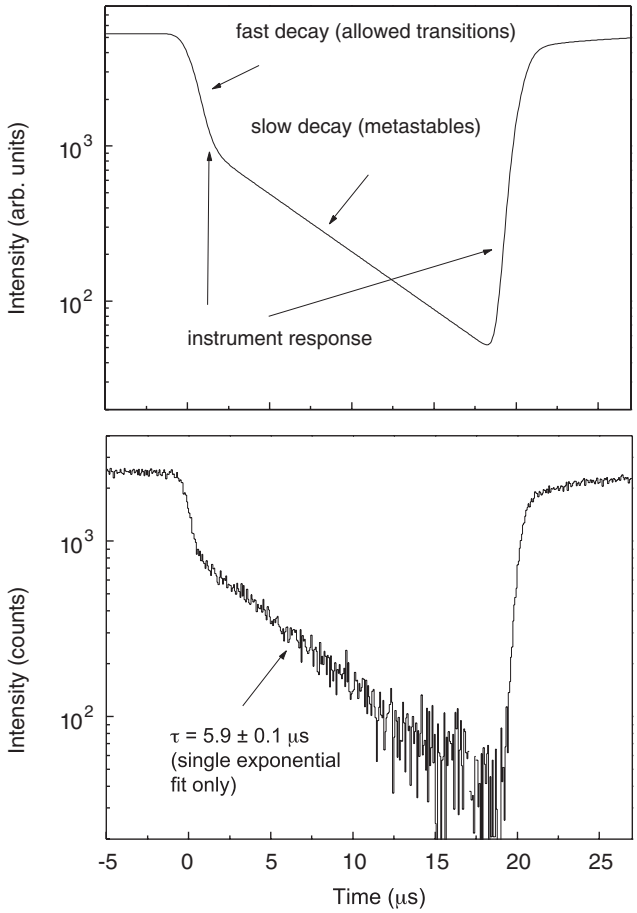

Figure 4. Comparison of the simulated time evolution of the emission intensity of the apparent $M2$ transition in neon-like Fe XVII with experimental data obtained with a Si(Li) detector. Electric-dipole transitions with fast decay rates account for the initial shoulder. Its width is determined by the time response and jitter of the detector and must be included in the model used to fit the decay curve. The inferred decay of 5.9 ± 0.1 μs from fitting a single exponential decay plus detector does not take into account contamination from the decay of the $(2s^22p^5_{1/2}3s_{1/2})_{J=0}$ level.

spectrometer. The position-sensitive gas proportional counter employed in this spectrometer has a rise time of several tens of

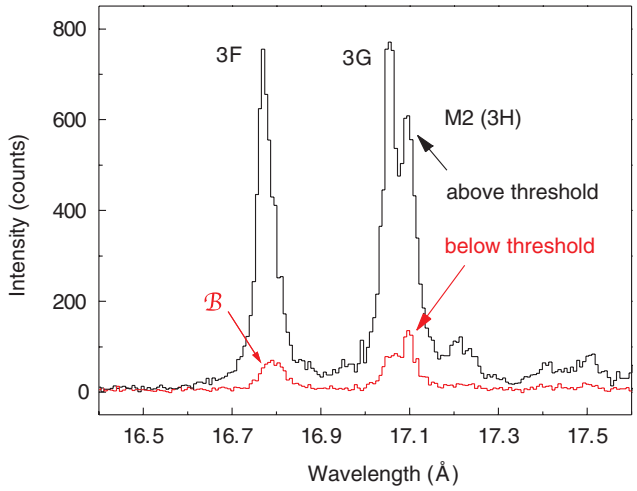

Figure 5. Spectra of the $2p^6$–$2p^5 3s$ transitions in neon-like Fe XVII recorded with a flat-crystal spectrograph. The beam energy is switched from a value above the threshold for direct excitation of the $2p^6$–$2p^5 3s$ transitions to a value well below. The spectrum after the switch is time integrated over 20 microseconds.
(A color version of this figure is available in the online journal.)

nanoseconds. The sudden step in the line intensity indicates that the direct excitation of the levels involved ceases in less than 60 ns after the pulse. The time resolution is higher than this, since the measured decay time corresponds to one time step of the analog-to-digital converter; a faster analog-to-digital converter setting showed a time resolution of <18 ns.

Figure 4 shows the time evolution of the signal detected with the Si(Li) detector. The Si(Li) detector has a much lower spectral resolution than the flat-crystal spectrometer, and its signal represents the integral of the $3 \rightarrow 2$ emission of Fe XVII. The slow rise time and poor time resolution of this type of detector reduce the slope of the prompt decay of the non-metastable levels. A simulation of the instrumental response based on a response function with a Gaussian profile $e^{(-t^2/w^2)}$ with $w = 530$ ns provides an excellent fit of the prompt decay and of the subsequent rise of the observed signal intensity as the beam energy resumes its original value. In addition, an exponential decay with a time constant of 5.9 μs provides an excellent fit to the experimental data, although, as we show in the next section, a single exponential decay does not adequately describe the physical processes.

4. EXPERIMENTAL RESULTS

In Figure 5, we present the spectrum obtained with the flat-crystal spectrometer while the electron beam energy is above the threshold for electron-impact excitation. The spectrum clearly shows the three strongest $3s \rightarrow 2p$ transitions, i.e., lines $3F$, $3G$, and $M2$. Additional features seen are from Fe XVI and possibly O VII, as described in detail by Graf et al. (2009). All three lines vanish and the spectrum is devoid of features, when the beam energy is set *permanently* to 630 eV, i.e., a value below the threshold for electron-impact excitation, or, of course, if the beam is permanently turned off. This assures that indeed no processes exist, which might lead to line formation at this energy. However, during the time when the beam is freshly switched from a value above the threshold to a value below, lines are clearly seen. This is also illustrated in Figure 5, where the time-integrated spectrum collected for a few tens of microseconds after switching the electron beam below the threshold is shown.

Casual inspection of the spectrum obtained after the beam is switched to below the threshold seems to indicate that the same three lines are still present. But more careful inspection shows that line $3F$ has vanished, as is expected from FAC calculations of its radiative decay rate of 7.82×10^{11} s^{-1}, which is way too fast to be resolved with our instrumentation. By the same reasoning, line $3G$ should have also vanished, as its radiative decay rate is 8.61×10^{11} s^{-1}, which is even faster than that associated with line $3F$. But, surprisingly, it is still seen. The reason is that its upper level is populated by the slow radiative decay from the $(2s^2 2p^5_{1/2} 3s_{1/2})_{J=0}$ level (cf. Figure 1). That level decays to the $(2s^2 2p^5_{3/2} 3s_{1/2})_{J=1}$ level (i.e., the upper level of line $3G$) via a magnetic dipole transition with a predicted rate of about 1.55×10^4 s^{-1}, resulting in a transition predicted by our FAC calculations to be at 1175 Å. This transition has been observed by the Solar Ultraviolet Measurement of Emitted Radiation instrument on board the *Solar and Heliospheric Observatory* mission, and its wavelength was measured to be 1153.151 ± 0.025 Å (Feldman et al. 2000).

The $(2s^2 2p^5_{1/2} 3s_{1/2})_{J=0}$ level is normally strictly forbidden to decay to the $(2s^2 2p^6)_{J=0}$ ground level because both levels have an angular momentum of zero. However, the presence of a magnetic field of sufficient strength induces Zeeman mixing of that level with the upper levels of lines $3F$ and $3G$ so that there is a finite probability that the $(2s^2 2p^5_{1/2} 3s_{1/2})_{J=0}$ level decays directly to the ground state emitting an X-ray transition (Beiersdorfer et al. 2003a). Following the earlier notation, we label the magnetic field induced X-ray transition $\mathcal{B}$ in the figure. We note that the present measurement is the first time that this line has been observed in the Fe XVII ion without blending with the $3F$ line.

The third line seen in the below-threshold spectrum in Figure 5 is $M2$. This is the line we expect to observe due to the slow radiative decay of its $(2s^2 2p^5_{3/2} 3s_{1/2})_{J=2}$ upper level. Resolving the below-threshold emission as a function of time in a second measurement in which the electron beam was turned off, we confirmed that the intensity of this line disappeared faster than that of $3G$ and $\mathcal{B}$. In this measurement, we extended the observation time to 180 μs after the beam energy was reduced. This is illustrated in Figure 6, where we show the emission summed during the time interval from 0 to 30 μs after the beam is turned off. In this spectrum, lines $M2$, $3G$, and $\mathcal{B}$ have about the same intensity. By contrast, the emission summed during the time 30 μs after the beam is switched shows a strongly reduced intensity of line $M2$.

The time evolution data of line $M2$ from the crystal spectrometer were fitted to yield a 5.5 ± 0.5 μs exponential decay. The small number of counts in these measurements determined the statistical error. The advantage of this measurement is that there is less contamination of the decay curve from the decay of the longer-lived $(2s^2 2p^5_{1/2} 3s_{1/2})_{J=0}$ level; however, because lines $M2$ and $3G$ are not fully resolved in the crystal spectrometer measurement, the decay of the $J = 0$ level still affects the measurement of the decay of the $J = 2$ level.

Since the Si(Li) detector recorded a much higher number of counts, a better determination of the decay constant is in principle possible by using those data, despite the intrinsically lower spectral resolution, as our determination presented above has already shown. In order to make the most accurate measurement, contamination of the observed radiative decay curve of the $M2$ line by the decay of the $(2s^2 2p^5_{1/2} 3s_{1/2})_{J=0}$ level must be accounted for. To do this we have recorded the $n = 3 \rightarrow n = 2$

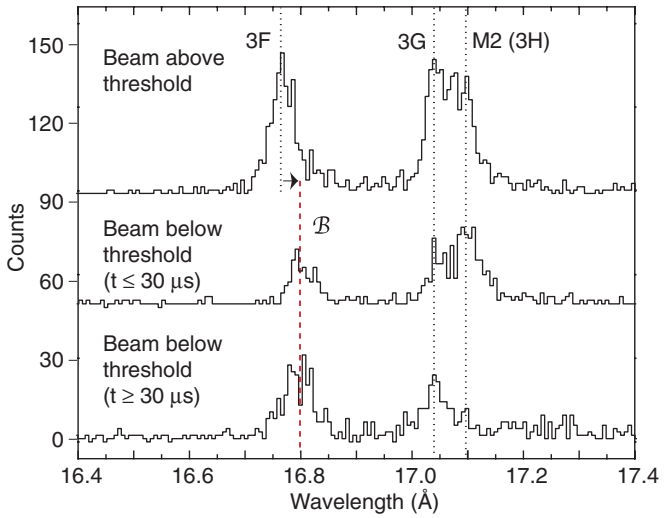

Figure 6. Spectra of the $2p^6$–$2p^5 3s$ transitions in neon-like Fe XVII recorded with a flat-crystal spectrograph. The beam energy is switched from a value above the threshold for direct excitation of the $M2$ ($3H$) transition to a value well below. Spectra shown were collected for different time periods before and after the switch. The difference in the positions of line $3F$ and of line $\mathcal{B}$ is clearly seen.

(A color version of this figure is available in the online journal.)

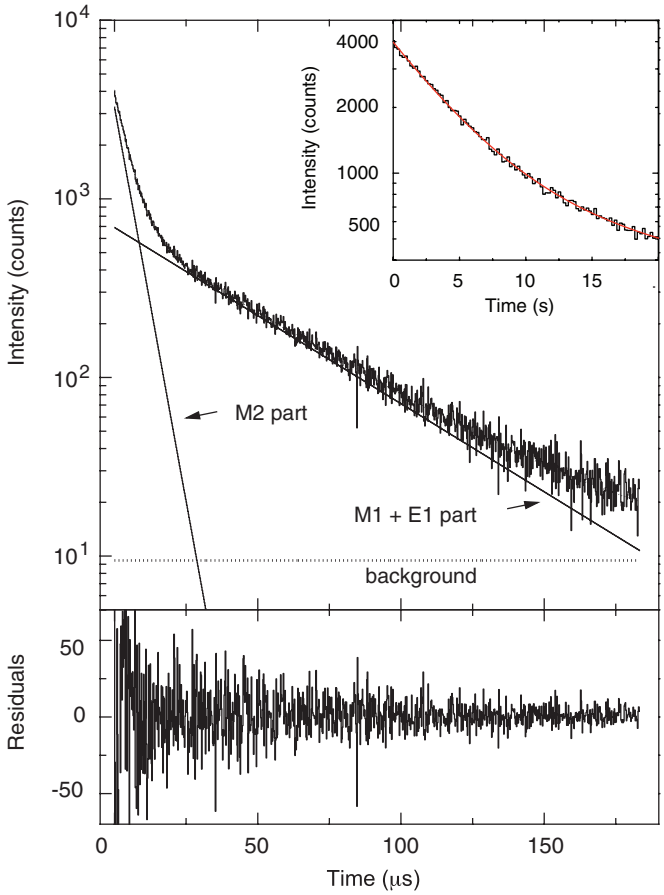

Figure 7. Time evolution of the emission of the spectrally unresolved $2p^6$–$2p^5 3s$ transitions in neon-like Fe XVII recorded with a Si(Li) detector. A multi-exponential fit reveals decay components from the magnetic quadrupole decay of the $(2s^2 2p^5_{3/2} 3s_{1/2})_{J=2}$ level and from the electric and magnetic dipole decay of the $(2s^2 2p^5_{1/2} 3s_{1/2})_{J=0}$ level as well as a constant background.

(A color version of this figure is available in the online journal.)

emission with the Si(Li) detector for 180 μs after the beam was switched off. The data are shown in Figure 7. Such a long observation time not only reveals the fast $M2$ decay, but also the slower decay of the $(2s^2 2p^5_{1/2} 3s_{1/2})_{J=0}$ level. Applying a two-exponential fit plus background to the observed decay curve results in a decay rate of 2.04×10^{-5} s^{-1} for the $M2$ line, corresponding to a lifetime of the $(2s^2 2p^5_{3/2} 3s_{1/2})_{J=2}$ level of 4.91 μs. The statistical error in the measured rate is 2×10^3 s^{-1} or 0.05 μs in the upper level lifetime. The accuracy of the timing fiducials of the data collection system is ± 0.04 μs and thus comparable to the statistical error. The main contribution ($-0.05/+0.22$ μs) to the fitting error of the decay of the $(2s^2 2p^5_{3/2} 3s_{1/2})_{J=2}$ level arises from how the residual background of the decay curve is fitted. In estimating this error, we chose to fit the data with different models assuming constant background, a time-varying background, or no background at all.

The final result of our measurement is $4.91^{+0.23}_{-0.07}$ μs for the radiative lifetime of the $(2s^2 2p^5_{3/2} 3s_{1/2})_{J=2}$ level, or $(2.04^{+0.03}_{-0.09}) \times 10^5$ s^{-1}. Here, we have combined the systematic and statistical errors in quadrature.

5. DISCUSSION

The radiative rates associated with the Fe XVII spectrum have been calculated by numerous authors, as shown in Table 1. The calculated rates range from 1.395×10^5 s^{-1} (Cornille et al. 1994) to 2.48×10^5 s^{-1} (Bhatia et al. 1985). Other calculated values lie in between (Bhatia & Doschek 1992; Bhatia & Saba 2001; Bhatia & Doschek 2003; Loulergue & Nussbaumer 1975; Nahar et al. 2003; Safronova et al. 2001).

Our own calculation using FAC 1.1.1 and a 37-level model yields a value of 2.063×10^5 s^{-1}, which in fact is remarkably close to the oldest available calculated value of 2.02×10^5 s^{-1} from Loulergue & Nussbaumer (1975). Indeed, these two calculated values are closest to our measured value of $(2.04^{+0.03}_{-0.09}) \times 10^5$ s^{-1}.

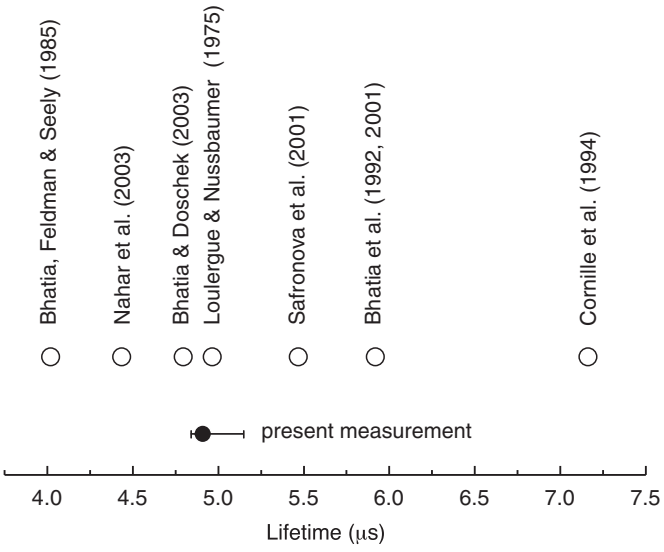

Figure 8. Comparison of measured and predicted values for the lifetime of the $(2s^2 2p^5_{3/2} 3s_{1/2})_{J=2}$ level in Fe XVII. For additional theory points see Table 1.

A graphical comparison between the calculated values found in the literature and our measurement is shown in Figure 8. Here, we have plotted the corresponding radiative lifetime of the upper level of the $M2$ transition in Fe XVII.

Our measurement of the radiative rates associated with the $M2$ transition is the first such measurement for the Fe XVII spectrum. The radiative rates of the many other transitions in the Fe XVII spectrum have yet to be checked by experiment. It is clear from our survey of calculated data that there are uncertainties in these rates of about a factor of 2. The overall uncertainties in the radiative rates thus cast doubt on the accuracy of the modeling of the Fe XVII spectrum, especially for lines such as the $M2$ transition, where radiative rates compete with either collisional or photoionization and photoexcitation processes. In those cases, the exact value of the radiative rates matters strongly. Further measurements of radiative rates will be needed to assess and remove these uncertainties from models of the Fe XVII spectrum.

P. B. gratefully acknowledges the help from Ming-Feng Gu in setting up and executing the Flexible Atomic Code. This work was supported by NASA's Astronomy and Physics Research and Analysis Program under work order NNG06WF08I and performed under the auspices of the US Department of Energy by the Lawrence Livermore National Laboratory under Contract DE-AC52-07NA27344.

REFERENCES

Behar, E., Cottam, J., & Kahn, S. M. 2001, ApJ, 548, 966
Beiersdorfer, P. 2003, ARA&A, 41, 343
Beiersdorfer, P. 2008, Can. J. Phys., 86, 1
Beiersdorfer, P., Bitter, M., von Goeler, S., & Hill, K. W. 2004, ApJ, 610, 616
Beiersdorfer, P., Scofield, J. H., & Osterheld, A. L. 2003a, Phys. Rev. Lett., 90, 235003
Beiersdorfer, P., Träbert, E., & Pinnington, E. H. 2003b, ApJ, 587, 836
Beiersdorfer, P., & Wargelin, B. J. 1994, Rev. Sci. Instrum., 65, 13
Beiersdorfer, P., et al. 1990, Phys. Rev. Lett., 65, 1995
Beiersdorfer, P., et al. 2002, ApJ, 576, L169
Bhatia, A. K., & Doschek, G. A. 1992, At. Data Nucl. Data Tables, 52, 1
Bhatia, A. K., & Doschek, G. A. 2003, At. Data Nucl. Data Tables, 85, 1
Bhatia, A. K., Feldman, U., & Seely, J. F. 1985, At. Data Nucl. Data Tables, 32, 435
Bhatia, A. K., & Saba, J. L. R. 2001, ApJ, 563, 434
Brenner, G., Crespo López-Urrutia, J. R., Harman, Z., Mokler, P. H., & Ullrich, J. 2007, Phys. Rev. A, 75, 032504
Brown, G. V. 2008, Can. J. Phys., 86, 199
Brown, G. V., Beiersdorfer, P., & Widmann, K. 2001, Phys. Rev. A, 63, 032719
Brown, I. G., Galvin, J. E., MacGill, R. A., & Wright, R. T. 1986, Appl. Phys. Lett., 49, 1019
Chen, G. X., Kirby, K., Silver, E., Brickhouse, N. S., Gillaspy, J. D., Tan, J. N., Pomeroy, J. M., & Laming, J. M. 2006, Phys. Rev. Lett., 97, 143201
Chen, G. X., Kirby, K., Silver, E., Brickhouse, N. S., Gillaspy, J. D., Tan, J. N., Pomeroy, J. M., & Laming, J. M. 2007, Phys. Rev. Lett., 99, 109902
Cornille, M., Dubau, J., Faucher, P., Bely-Duabu, F., & Blanchard, C. 1994, A&AS, 105, 77
Crespo López-Urrutia, J. R., Beiersdorfer, P., Savin, D. W., & Widmann, K. 1998, Phys. Rev. A, 58, 238
Crespo López-Urrutia, J. R., Beiersdorfer, P., & Widmann, K. 2006, Phys. Rev. A, 74, 012507
Feldman, U., Curdt, W., Landi, E., & Wilhelm, K. 2000, ApJ, 544, 508
Graf, A. T., Beiersdorfer, P., Brown, G. V., & Gu, M. F. 2009, ApJ, 695, 818
Gu, M. F. 2008, Can. J. Phys., 86, 675
Gu, M. F. 2009, arXiv:0905.0519
Gu, M.-F., et al. 2004, ApJ, 607, L143
Laming, J. M., et al. 2000, ApJ, 545, L161
Lapierre, A., et al. 2005, Phys. Rev. Lett., 95, 183001
Levine, M. A., et al. 1989, Nucl. Instrum. Methods, B43, 431
Loulergue, M., & Nussbaumer, H. 1973, A&A, 24, 209
Loulergue, M., & Nussbaumer, H. 1975, A&A, 45, 125
Mauche, C. W., Liedahl, D. A., & Fournier, K. B. 2001, ApJ, 560, 992
Mauche, C. W., Liedahl, D. A., & Fournier, K. B. 2005, in AIP Conf. Ser. 774, X-ray Diagnostics of Astrophysical Plasmas: Theory, Experiment, and Observation, ed. R. Smith (Melville, NY: AIP), 133
Nahar, S. N., Eissner, W., Chen, G.-X., & Pradhan, A. K. 2003, A&A, 408, 789
Neill, P., Beiersdorfer, P., Brown, G., Harris, C., Träbert, E., Utter, S. B., & Wong, K. L. 2000, Phys. Scr. A, 62, 141
Ness, J.-U., Schmitt, J. H. M. M., Audard, M., & Güdel, Mewe R. 2003, A&A, 407, 347
Paerels, F. B. S., & Kahn, S. M. 2003, ARA&A, 41, 291
Parkinson, J. H. 1973, A&A, 24, 215
Safronova, U. I., Namba, C., Murakami, I., Johnson, W. R., & Safronova, M. S. 2001, Phys. Rev. A, 64, 012507
Smith, B. W., Raymond, J. C., Mann, J. B., & Cowan, R. D. 1983, ApJ, 298, 898
Stefanelli, G. S., Beiersdorfer, P., Decaux, V., & Widmann, K. 1995, Phys. Rev. A, 52, 3651
Träbert, E. 2002, Phys. Scr., 100T, 88
Träbert, E. 2008, Can. J. Phys., 86, 73
Träbert, E., Beiersdorfer, P., Brown, G. V., Smith, A. J., Utter, S. B., Gu, M. F., & Savin, D. W. 1999, Phys. Rev. A, 60, 2034
Träbert, E., et al. 2000, ApJ, 541, 506
Wargelin, B. J., Beiersdorfer, P., & Kahn, S. M. 1993, Phys. Rev. Lett., 71, 2196
Xu, H., Kahn, S. M., Peterson, J. R., Behar, E., Paerels, F. B. S., Mushotzky, R. F., Jernigan, J. G., & Makishima, K. 2002, ApJ, 579, 600